



ELSEVIER

Contents lists available at SciVerse ScienceDirect

Journal of Sound and Vibration

journal homepage: www.elsevier.com/locate/jsvi

Rapid Communications

Metadamping: An emergent phenomenon in dissipative metamaterials



Mahmoud I. Hussein*, Michael J. Frazier

Department of Aerospace Engineering Sciences, University of Colorado Boulder, Boulder, CO 80309, USA

ARTICLE INFO

Article history:

Received 16 July 2012

Received in revised form

11 April 2013

Accepted 24 April 2013

Handling Editor: G. Degrande

Available online 29 May 2013

ABSTRACT

Using a generalized form of Bloch's theorem, we derive the dispersion relation of a viscously damped locally resonant metamaterial modeled as an infinite mass-in-mass lumped parameter chain. For comparison, we obtain the dispersion relation for a statically equivalent Bragg-scattering mass-spring chain that is also viscously damped. For the two chains, we prescribe identical damping levels in the dashpots and compare the damping ratio associated with all propagating Bloch modes. We find that the locally resonant metamaterial exhibits higher dissipation throughout the spectrum which indicates a damping emergence phenomena due to the presence of local resonance. This phenomenon, which we define as “metadamping”, provides a new paradigm for the design of material systems that display both high damping and high stiffness. We conclude our investigation by quantifying the degree of metadamping as a function of the long-wave speed of sound in the medium or the static stiffness.

© 2013 Elsevier Ltd. All rights reserved.

1. Introduction

Damping is an intrinsic property of materials and when present in a structural configuration may play a significant role in shaping the structural response. While in certain applications—such as energy harvesting—dissipation is not desired, its maximization is sought in numerous avenues, including vibration suppression, shock resistance, and acoustic absorption. From a design perspective, a highly constraining trade-off in these latter applications is that an increase in the intensity of damping in the materials employed commonly appears at the expense of stiffness, or mechanical load-bearing capacity. For example, elastomeric materials are more dissipative than metallic materials but are much less stiff. Hence, the development of concepts in material design that lead to both high levels of dissipation and stiffness has been an active area of research. Lakes et al. [1], for example, demonstrated that composite materials incorporating constituents in a metastable state simultaneously exhibit elevated values of viscoelastic stiffness and damping. Research on shape memory alloys has also presented an example, showing that hysteretic motion of interfaces at the thermoelastic martensitic phase leads to realization of high damping capacity without reduction in overall stiffness [2]. Chung [3] presents a review of other approaches for enhancing damping-stiffness capacity of materials through composite materials engineering.

In this Communication, we propose periodic acoustic metamaterials (AMs) with local resonance properties [4] as a candidate for materials that can be designed to exhibit high levels of dissipation while retaining high stiffness. An underlying principle is that vibration attenuation due to damping is most profound at resonance frequencies, as is well

* Corresponding author. Tel.: +1 3034923177.

E-mail address: mih@colorado.edu (M.I. Hussein).

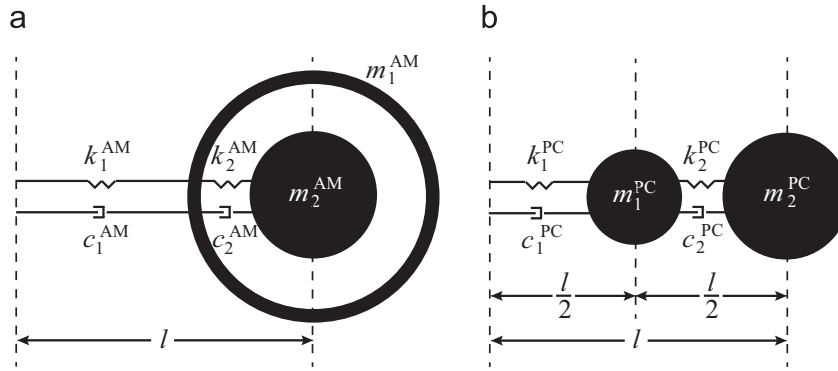


Fig. 1. Unit cells of statically-equivalent periodic chains consisting of masses, springs and viscous damping (dashpot) elements: (a) acoustic metamaterial (mass-in-mass), (b) phononic crystal (mass-and-mass).

known in the field of structural dynamics. Here we draw an analogy and explore the effect of resonance on dissipation in the context of what we may refer to as “material dynamics”. In this setting, we examine the level of dissipation not only near a resonance frequency but across the entire frequency-wavenumber spectrum of the material’s dispersion curves.

To assess the degree of dissipation in a locally resonant AM, we first generalize Bloch’s theorem to incorporate complex frequencies—which is necessary to allow for proper treatment of temporally attenuating waves.¹ We then derive the frequency and damping ratio band structures of a damped AM and compare the characteristics of the latter with those of a corresponding statically-equivalent phononic crystal (PC), i.e., another type of periodic material that does not possess local resonances yet has the same long-wave propagation characteristics. In this analysis, we seek to determine the possibility of an “emergence of damping” in the AM. The concept of emergence in complex systems theory and other disciplines stems from the widely held notion that for certain systems “the whole is greater than the sum of its parts” [6]. Although emergence is usually associated with a lack of predictability, the concept may also be relevant to systems whose properties are predictable in principle, yet unforeseen *a priori* [7]. In relation to chemistry and materials science, often the emerging *whole* stems from the structure while the *parts* is associated with the composition. From a similar perspective, our aim is to demonstrate emergence in the context of how local resonance within the internal structure, of a material, leads to enhanced dissipation, over all frequencies and wavenumbers, when compared to other materials with equivalent static properties and the same level of prescribed damping. We emphasize that the practical implications of damping emergence are profound since this phenomenon provides a novel paradigm towards the design of materials with both high damping and high stiffness.

2. Acoustic metamaterial and phononic crystal: Models and equations of motion

By considering lumped masses, springs, and viscous damping (dashpot) elements, we construct a simple one-dimensional (1D) model of a damped diatomic AM (represented by a “mass-in-mass” configuration [8] as shown in Fig. 1a), and for comparison we also examine a corresponding 1D model of a damped diatomic PC (represented by a “mass-and-mass” configuration as shown in Fig. 1b). This choice of simple lumped parameter models allows us to focus on the underlying damping emergence phenomenon free from the distraction of irrelevant system complexities. Both models represent a unit cell that is infinitely repeated in both directions.

Considering unit cell periodicity, the set of homogeneous equations describing the motion of each mass in the AM model shown in Fig. 1a is obtained as follows (where the AM superscript is omitted for brevity):

$$\begin{aligned} m_1 \ddot{u}_1^j + c_1(2\dot{u}_1^j - \dot{u}_1^{j-1} - \dot{u}_1^{j+1}) + c_2(\dot{u}_1^j - \dot{u}_2^j) + k_1(2u_1^j - u_1^{j-1} - u_1^{j+1}) + k_2(u_1^j - u_2^j) &= 0, \\ m_2 \ddot{u}_2^j + c_2(\dot{u}_2^j - \dot{u}_1^j) + k_2(u_2^j - u_1^j) &= 0, \end{aligned} \quad (1)$$

where u_α^j is the displacement of mass α in an arbitrary j th unit cell. In general, a unit cell and its neighbors may be identified by $j+n$, where $n=0, -1, 1$ denotes the present, previous, and subsequent unit cell, respectively. Similarly for the PC model shown in Fig. 1b, the equations of motion corresponding to the two masses are (where the PC superscript is omitted for brevity) as follows:

$$\begin{aligned} m_1 \ddot{u}_1^j + (c_1 + c_2)\dot{u}_1^j - c_2\dot{u}_2^j - c_1\dot{u}_2^{j-1} + (k_1 + k_2)u_1^j - k_2u_2^j - k_1u_2^{j-1} &= 0, \\ m_2 \ddot{u}_2^j + (c_1 + c_2)\dot{u}_2^j - c_2\dot{u}_1^j - c_1\dot{u}_1^{j+1} + (k_1 + k_2)u_2^j - k_2u_1^j - k_1u_1^{j+1} &= 0. \end{aligned} \quad (2)$$

¹ The original form of Bloch’s theorem, which was developed for electronic band structure calculation [5], is sufficiently based on real frequencies.

3. Generalized Bloch's theorem: Derivation of frequency and damping ratio dispersion curves

For each of the system of equations, Eqs. (1) and (2), we apply the generalized form of Bloch's theorem [9,10]

$$u_{\alpha}^{j+n}(x, \kappa; t) = \tilde{U}_{\alpha} e^{i(\kappa x_{\alpha}^j + n\kappa l) + \lambda t}, \quad \alpha = 1, 2, \quad (3)$$

(where $x_{\alpha}^j = j + l$ for the AM model and $x_{\alpha}^j = j + \alpha l/2$ for the PC model) which represents the displacement of mass α in the $(j+n)$ th unit cell in the periodic chain, and where \tilde{U}_{α} is the wave amplitude, l is the unit-cell length, κ is the wavenumber and λ is a complex frequency function that permits wave attenuation in time. In the limiting case of no damping, $\lambda = \pm i\omega$, and the usual form of Bloch's theorem is recovered. Substituting Eq. (3) into the governing equations for both the AM and the PC yields a characteristic equation of the form

$$\lambda^4 + a\lambda^3 + b\lambda^2 + c\lambda + d = 0, \quad (4)$$

where for the AM,

$$\begin{aligned} a &= \frac{(m_1 + m_2)c_2 + 2m_2c_1(1 - \cos \kappa l)}{m_1 m_2}, \\ b &= \frac{(m_1 + m_2)k_2 + 2(m_2k_1 + c_1c_2)(1 - \cos \kappa l)}{m_1 m_2}, \\ c &= \frac{2(c_1k_2 + c_2k_1)(1 - \cos \kappa l)}{m_1 m_2}, \\ d &= \frac{2k_1k_2(1 - \cos \kappa l)}{m_1 m_2}, \end{aligned} \quad (5)$$

and for the PC,

$$\begin{aligned} a &= \frac{(m_1 + m_2)(c_1 + c_2)}{m_1 m_2}, \\ b &= \frac{(m_1 + m_2)(k_1 + k_2) + 2c_1c_2(1 - \cos \kappa l)}{m_1 m_2}, \\ c &= \frac{2(c_1k_2 + c_2k_1)(1 - \cos \kappa l)}{m_1 m_2}, \\ d &= \frac{2k_1k_2(1 - \cos \kappa l)}{m_1 m_2}. \end{aligned} \quad (6)$$

We note that the form of each of c and d does not vary between the two models. Upon solving Eq. (4) for either the AM or the PC, we obtain the general solution

$$\lambda_{1,2} = \frac{1}{12} \left(3a \mp \sqrt{9a^2 - 24b + 6\sqrt[3]{4P} + \frac{12\sqrt[3]{2Q}}{P}} + \sqrt{18a^2 - 48b - 6\sqrt[3]{4P} - \frac{12\sqrt[3]{2Q}}{P} \mp \frac{54(a^3 - 4ab + 8c)}{\sqrt{9a^2 - 24b + 6\sqrt[3]{4P} + \frac{12\sqrt[3]{2Q}}{P}}} \right) \quad (7a)$$

where

$$Q = b^2 - 3ac + 12d, \quad (7b)$$

$$P = \sqrt[3]{2b^3 - 9abc + 27(c^2 + a^2d) - 72bd} + \sqrt{-4Q^3 + [2b^3 - 9abc + 27(c^2 + a^2d) - 72bd]^2}. \quad (7c)$$

The distinction between the solution of the two systems arises upon the appropriate substitution of a and b as given in Eqs. (5) and (6), respectively.

The roots we obtain from Eq. (7) may also be expressed as

$$\lambda_s(\kappa) = -\xi_s(\kappa)\omega_s(\kappa) \pm i\omega_{d_s}(\kappa), \quad s = 1, 2, \quad (8)$$

where s represents the branch number. Hence from Eqs. (7) and (8), we can obtain the frequency, $\omega_{d_s}(\kappa)$, and damping ratio, $\xi_s(\kappa)$, relations. Specifically, from the complex solution, $\lambda_s(\kappa)$, we directly extract $\omega_{d_s}(\kappa) = \text{Im}[\lambda_s(\kappa)]$ and $\xi_s(\kappa) = -\text{Re}[\lambda_s(\kappa)] / \text{Abs}[\lambda_s(\kappa)]$ for each of the two dispersion branches.

4. Metadamping phenomenon

Now we examine the frequency and damping ratio dispersion curves of both systems for the following parameter ratios: $m_2^{\text{AM}}/m_1^{\text{AM}} = m_2^{\text{PC}}/m_1^{\text{PC}} = 5$ and $k_2^{\text{AM}}/k_1^{\text{AM}} = k_2^{\text{PC}}/k_1^{\text{PC}} = 1/5$. Furthermore, we set $m_1^{\text{AM}} = m_1^{\text{PC}} = 1$, $\omega_0^{\text{PC}} = \sqrt{k_2^{\text{PC}}/m_2^{\text{PC}}} = 100$ and $l = 1$. All the parameters here and elsewhere in this work may be read in any consistent system of physical units. To enable proper

comparison, we select the value of $\omega_0^{AM} = \sqrt{k_2^{AM}/m_2^{AM}}$ in such a manner as to render both systems statically equivalent, that is, both systems having the same long-wave sound speed, or slope of the first frequency dispersion branch as the wavenumber tends to zero, $c_{stat} = \lim_{\kappa \rightarrow 0} \omega_{d_1}/\kappa$. With the chosen parameters for the PC, $c_{stat} = 83.33$. The AM is set to exhibit the same value of long-wave sound speed when $\omega_0^{AM} = 40.90$. Concerning the damping prescription, we define $\eta_1 = c_1^{PC} = c_1^{AM}$ and $\eta_2 = c_2^{PC} = c_2^{AM}$. For the special case of the two dashpots in each system having the same prescribed damping value, we define $\eta = \eta_1 = \eta_2$ (i.e., $c_2^{AM}/c_1^{AM} = c_2^{PC}/c_1^{PC} = 1$).

The first set of results is shown in Fig. 2. The left hand side (LHS) of Fig. 2a displays the frequency band structure of the AM for three example cases: no damping ($\eta=0$), low damping ($\eta=40$), and high damping ($\eta=80$), and the LHS of Fig. 2b and c displays the damping ratio band structures for the low damping and high damping cases, respectively. In the damping ratio diagrams, we have added a third curve to represent the summation of the damping ratio values for the acoustic and optical branches, i.e., $\xi_{sum}(\kappa)_r = \xi_1(\kappa)_r + \xi_2(\kappa)_r$, where $r=AM$ or PC. On the right hand side (RHS) of Fig. 2, the matching diagrams for the corresponding PC are shown. The results show that there are shifts in the frequency band diagrams (greater in the optical branches) due to the presence of damping, and that these shifts are more profound in the AM. This behavior manifests itself in a most remarkable manner in the damping ratio diagrams. Despite the static equivalence and equally prescribed value of the viscous damping constant, η , we observe in Fig. 2b and c that the AM exhibits higher damping ratio values (i.e., higher dissipation) across the entire Brillouin zone (BZ), for both the acoustic and optical branches. This is an indication of a considerable amplification, or emergence, of dissipation in the AM compared to its PC counterpart. Moreover, this emergence is present for all propagating Bloch modes and not only for modes close to the band gap. Consequently, even though the band gap of the AM might be smaller in width, as in our case, the overall wave attenuation performance when viewed across the entire spectrum is more favorable compared to the PC. This is because outside a band gap, attenuation of propagating modes may only be realized via damping.

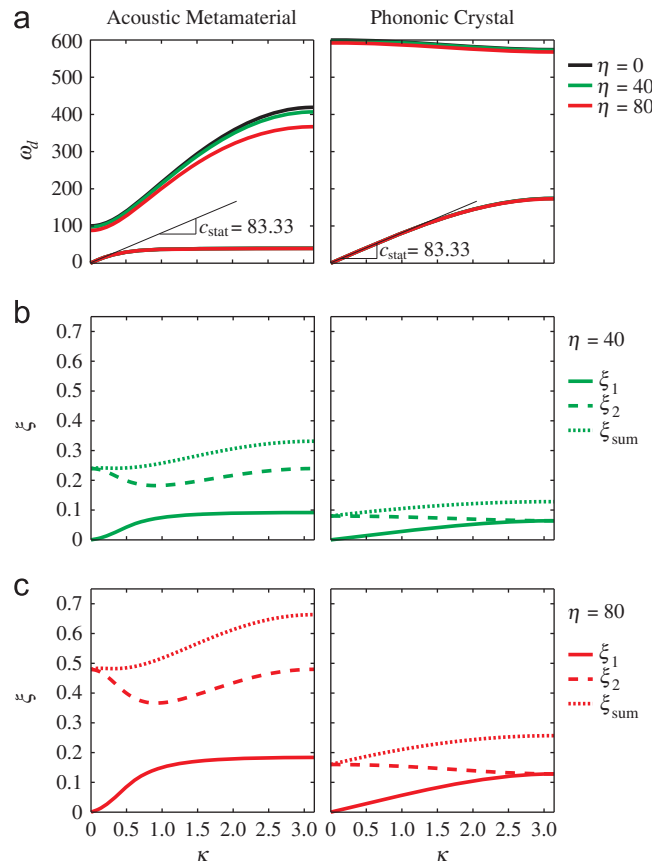


Fig. 2. (a) Frequency band structure; for each branch, the top set of curves represent no damping, the intermediate set represents $\eta=40$ and the bottom set represents $\eta=80$. Damping ratio band structure corresponding to (b) $\eta=40$ and (c) $\eta=80$. In all sub-figures, the LHS corresponds to AM and the RHS corresponds to statically equivalent PC.

To quantify this difference in damping ratio values, we introduce a wavenumber-dependent *damping emergence metric*, $Z_l(\kappa) = \xi_l(\kappa)|_{AM} - \xi_l(\kappa)|_{PC}$, where $l=1,2$ or sum. In Fig. 3, we show $Z_l(\kappa)$, its cumulative value

$$Z_l^{cum}(\theta) = \int_0^\theta Z_l d\kappa, \quad l = 1, 2 \text{ or sum}; \quad \theta \in [0, \pi], \quad (9)$$

and its total value, $Z_l^{tot} = Z_l^{cum}(\pi)$ for our example AM and PC pair—displaying the data for the acoustic branch ($l=1$), the optical branch ($l=2$), and the summation of the two branches ($l=\text{sum}$) in Fig. 3a–c, respectively (for $\eta=40$ on the LHS and $\eta=80$ on the RHS). The results reveal significantly high values of Z_l^{tot} which we may view as a measure of the intensity of damping emergence. We also observe that $Z_2 > Z_1$ for all values of κ , in line with what we noted above. Fig. 4a shows that the value of Z_l^{tot} varies linearly with the level of damping, η . Here the subfigure terminates when the value of the damping ratio of the AM optical branch is no longer limited to unity (i.e., critical damping) within the BZ. This occurs at $\eta=165.57$. Fig. 4b focuses on isolating the role of c_1^{AM} versus c_2^{AM} in the creation of damping emergence (considering that only c_2^{AM} is associated with the prescribed damping level of the local resonator in the AM). This is done by varying η_2 while keeping $\eta_1=0$ and comparing with the case of varying η_1 while keeping $\eta_2=0$. The case of varying η (i.e., varying η_1 and η_2 simultaneously while keeping them equal) is also plotted for reference. A more representative reference curve is one that corresponds to varying $\eta/2$, as it directly correlates with the first two curves since the total amount of prescribed damping among the two dashpots is the same for each value of η^* . As expected, it is shown that the impact of c_2^{AM} is higher than that of c_1^{AM} , although not by a significant degree. This suggests that prescribed damping levels even away from local resonators in an AM are bound to influence damping emergence.

Returning to the driving objective of realizing materials that exhibit increased damping without deterioration of static stiffness, we repeat our calculations for a range of c_{stat} values. We do so by keeping all the parameters as in the previous

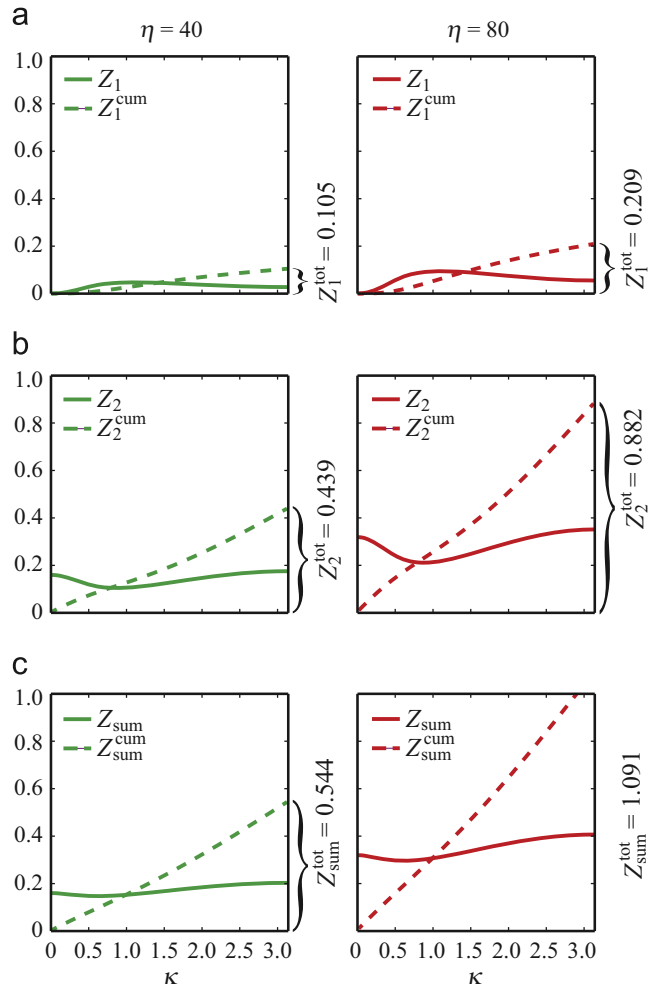


Fig. 3. Damping emergence metric, Z_l , for (a) acoustic branch ($l=1$), (b) optical branch ($l=2$), and (c) summation of the two branches ($l=\text{sum}$), for $\eta=40$ (LHS) and $\eta=80$ (RHS). The cumulative value, Z_l^{cum} (as defined in Eq. (9)), is also plotted, and the total value, Z_l^{tot} , is marked for each of the $\eta=40$ and $\eta=80$ cases. All results are for $c_{stat}=83.33$.

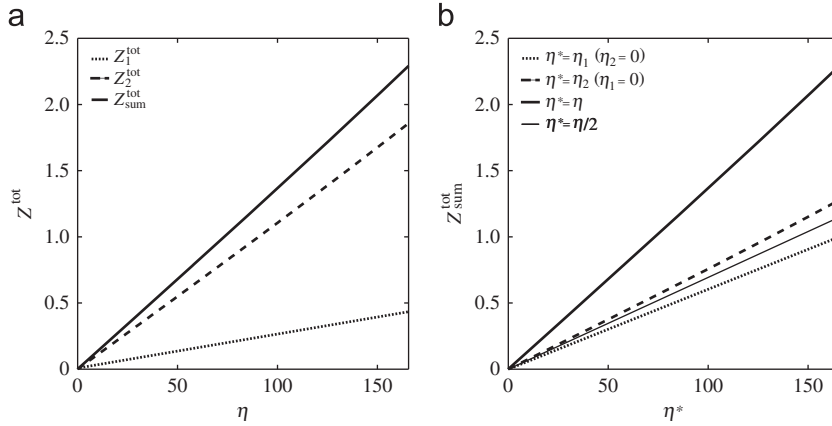


Fig. 4. (a) Total damping emergence, Z^{tot} , versus intensity of prescribed damping, η , for the acoustic branch ($l=1$), optical branch ($l=2$), and summation of the two branches ($l=\text{sum}$). (b) Total damping emergence summed over the two branches, $Z_{\text{sum}}^{\text{tot}}$, versus intensity of prescribed damping, η^* , considering the cases of varying the prescribed damping level in only the first dashpot ($\eta^* = \eta_1$), only the second dashpot ($\eta^* = \eta_2$), and both dashpots together ($\eta^* = \eta$ or $\eta^* = \eta/2$). Results are for $c_{\text{stat}} = 83.33$.

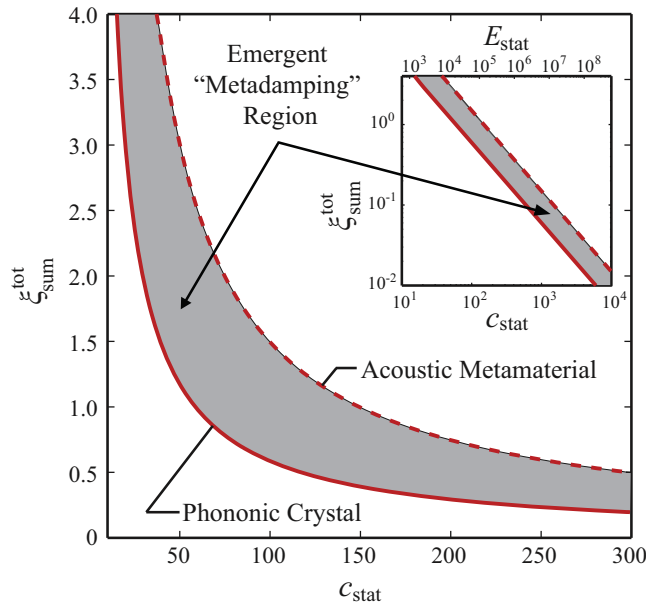


Fig. 5. Graphical illustration of metadamping: total damping ratio over the two branches, $\xi_{\text{sum}}^{\text{tot}}$, versus long-wave speed of sound, c_{stat} , in the periodic chains for $\eta = 80$. The solid and dashed lines correspond to PC and AM, respectively. The shaded gray region represents the region of damping emergence. In the inset, the same plot is reproduced in a log–log scale covering a wider range of c_{stat} values. For further insight, another scale is added showing an effective static Young’s modulus, E_{stat} , for an equivalent rod with unit cross-sectional area. The values of E_{stat} are dependent on our selection of $m_1^{\text{PC}} = m_1^{\text{AM}} = 1$; upon selection of heavier masses, E_{stat} will increase accordingly.

example except for ω_0^{PC} and ω_0^{AM} . Changing ω_0^{PC} causes c_{stat} to vary, and, in turn, ω_0^{AM} is adjusted accordingly to keep both systems statically equivalent. Throughout this process, the ratio $\omega_0^{\text{AM}}/\omega_0^{\text{PC}}$ stays constant, and hence the relative size and location of the undamped band gap between one system and the other also remains constant. In Fig. 5, we show the relationship between the level of dissipation (i.e., actual damping) versus c_{stat} for the AM and the PC. For this purpose, we calculate the total damping ratio over both branches, $\xi_{\text{sum}}^{\text{tot}}$, which we obtain by integration, i.e., $\xi_{\text{sum}}^{\text{tot}} = \xi_{\text{sum}}^{\text{cum}}(\pi)$, where

$$\xi_{\text{sum}}^{\text{cum}}(\theta) = \int_0^\theta \xi_{\text{sum}} \, d\kappa; \quad \theta \in [0, \pi]. \tag{10}$$

To provide further insight, we calculate an effective static Young’s modulus, E_{stat} , which we obtain by considering an effective elastic rod, with a cross-sectional area equal to unity. Using the standard rod properties of E , the Young’s modulus, ρ , the density, and $c = \sqrt{E/\rho}$, the speed of sound in the rod, we derive $E_{\text{stat}} \approx (m_1^r + m_2^r)c_{\text{stat}}^2$, where $r = \text{AM}$ or PC , for each of our periodic chains. We clearly observe in Fig. 5 that for a given value of long-wave speed, or effective static Young modulus,

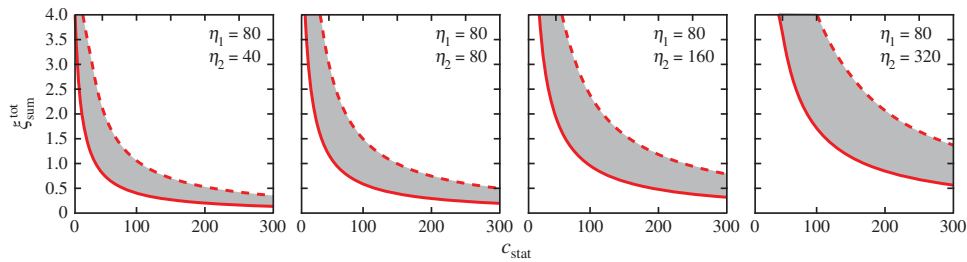


Fig. 6. Evolution of metadamping strength with increase in η_2 while keeping η_1 constant. The solid and dashed lines correspond to PC and AM, respectively. The second subfigure from the left corresponds to the $\eta=80$ case shown in Fig. 5 and presented again here as a reference case.

the AM exhibits a substantial increase in the value of $\xi_{\text{sum}}^{\text{tot}}$, when compared to the PC. In other words, even though there is still a trade-off between damping and stiffness, the level of dissipation in the AM increases without sacrifice of stiffness. Shaded in gray is the region of damping emergence, or “metadamping region”. We note that the level of metadamping (represented by the height of the shaded region) is highest at low levels of c_{stat} (i.e., compliant materials) and reduces in value as c_{stat} increases to represent more stiff materials. The intensity of metadamping, or area of the metadamping region, increases with η , or η_1 and η_2 (as we may deduce from Fig. 4 and as elaborately demonstrated in Fig. 6); however, for a given η , or η_1 and η_2 , this area may be increased further upon optimization of the periodic chain parameters including the local resonator parameters [11].

5. Conclusions

In conclusion, we have demonstrated the concept of damping emergence, or metadamping, due to the presence of local resonance. This finding has far reaching implications on the design of materials for numerous applications that require the reduction, mitigation, or absorption of vibrations, shock, and/or sound. While the analysis has been presented in the context of simple mass-spring-dashpot periodic chains, it can be readily extended to practical realizations of locally resonant acoustic metamaterials. Examples include material structures that utilize: heavy inclusions with compliant coatings [4], soft inclusions [12], split-resonators [13], inertial amplifiers [14], pillars [15,16], holey cylinders [17] and suspended masses [18]. The two underlying features needed are (1) the presence of locally resonant elements and (2) the presence of at least one constituent material phase or component that exhibits damping (e.g., by utilizing viscoelastic materials, friction at material interfaces, etc.). It is the combination of these two features that forms a prerequisite for metadamping. As such, other concepts for enhancing damping while retaining stiffness (such as those described in Refs. [1–3]) may be applied in conjunction with the inclusion of local resonators leading to an additive effect. While the perspective in this study has been that metadamping is a desired phenomenon (i.e., for the applications noted above), conversely, there is another category of metamaterial-based applications where metadamping is not desired (such as subwavelength energy harvesting, waveguiding or focusing). For this latter category, however, an awareness and understanding of the phenomenon is necessary for achievement of optimal design. Finally, while the concept of metadamping has been presented in the context of a mechanical problem, in principle it is also applicable to other disciplines in materials physics that involve both resonance and dissipation.

Acknowledgment

This work has been partially supported by the DARPA Young Faculty Award program (Grant number: YFA N66001-11-1-4134) and the NSF Graduate Research Fellowship program (Award number: DGE 1144083).

References

- [1] R.S. Lakes, T. Lee, A. Bersie, Y.C. Wang, Extreme damping in composite materials with negative-stiffness inclusions, *Nature* 410 (2001) 565–567.
- [2] J. Van Humbeeck, Damping capacity of thermoelastic martensite in shape memory alloys, *Journal of Alloys and Compounds* 355 (2003) 58–64.
- [3] D.D.L. Chung, Structural composite materials tailored for damping, *Journal of Alloys and Compounds* 355 (2003) 216–223.
- [4] Z.Y. Liu, X.X. Zhang, Y.W. Mao, Y.Y. Zhu, Z.Y. Yang, C.T. Chan, P. Sheng, Locally resonant sonic materials, *Science* 289 (2000) 1734–1736.
- [5] F. Bloch, Über die quantenmechanik der elektronen in kristallgittern [On the quantum mechanics of the electron in crystal lattices], *Zeitschrift für Physik* 52 (1928) 555–600.
- [6] J. Goldstein, Emergence as a construct: history and issues, *Emergence* 1 (1999) 49–72.
- [7] P.L. Luisi, Emergence in chemistry: Chemistry as the embodiment of emergence, *Foundations of Chemistry* 4 (2002) 183–200.
- [8] H.H. Huang, C.T. Sun, G.L. Huang, On the negative effective mass density in acoustic metamaterials, *International Journal of Engineering Science* 47 (2009) 610–617.
- [9] M.I. Hussein, Theory of damped Bloch waves in elastic media, *Physical Review B* 80 (2009) 212301.
- [10] M.I. Hussein, M.J. Frazier, Band Structures of Phononic Crystals with General Damping, *Journal of Applied Physics* 108 (2010) 093506.
- [11] M. Zilletti, S.J. Elliott, E. Rustighi, Optimisation of dynamic vibration absorbers to minimise kinetic energy and maximize internal power dissipation, *Journal of Sound and Vibration* 331 (2012) 4093–4100.

- [12] G. Wang, X.S. Wen, J.-H. Wen, L.-H. Shao, Y.-Z. Liu, Two-dimensional locally resonant phononic crystals with binary structures, *Physical Review Letters* 93 (2004) 154302.
- [13] A.B. Movchan, S. Guenneau, Split-ring resonators and localized modes, *Physical Review B* 70 (2004) 125116.
- [14] C. Yilmaz, G.M. Hulbert, N. Kikuchi, Phononic band gaps induced by inertial amplification in periodic media, *Physical Review B* 76 (2007) 054309.
- [15] Y. Pennec, B. Djafari-Rouhani, H. Larabi, J.O. Vasseur, A.C. Hladky-Hennion, Low-frequency gaps in a phononic crystal constituted of cylindrical dots deposited on a thin homogeneous plate, *Physical Review B* 78 (2008) 104105.
- [16] T.T. Wu, Z.-G. Huang, T.-C. Tsai, T.-C. Wu, Evidence of complete band gap and resonances in a plate with periodic stubbed surface, *Applied Physics Letters* 93 (2008) 111902.
- [17] J. Zhu, J. Christensen, J. Jung, L. Martin-Moreno, X. Yin, L. Fok, X. Zhang, F.J. Garcia-Vidal, A holey-structured metamaterial for acoustic deep-subwavelength imaging, *Nature Physics* 7 (2011) 52–55.
- [18] L. Liu, M.I. Hussein, Wave motion in periodic flexural beams and characterization of the transition between Bragg scattering and local resonance, *Journal of Applied Mechanics* 79 (2012) 011003.